行政院國家科學委員會專題研究計畫 期中進度報告

階層性自組裝嵌段共聚物-生物分子系統之研究--子計畫一：不同結構形態嵌段共聚高分子之合成及其與雙親性小分子之摻合研究(2/3)

期中進度報告(精簡版)

計 畫 類 別 ： 整合型
計 畫 編 號 ： NSC 95-2221-E-002-153-
執 行 期 間 ： 95 年 08 月 01 日至 96 年 07 月 31 日
執 行 單 位 ： 國立臺灣大學化學工程學系暨研究所

計 畫 主 持 人 ： 陳文章

處 理 方 式 ： 期中報告不提供公開查詢

中 華 民 國 96 年 05 月 29 日

行政院國家科學委員會補助專題研究計畫□ 成 果 報 告
■ 期中進度報告

階層性自組裝嵌段共聚物-生物分子系統之研究--子計畫一：不同結構形態嵌段共聚高分子之合成及其與雙親性小分子之摻合研究(2/3)

計畫類別：□個別型計畫　　■ 整合型計畫
計畫編號： NSC-95-2221-E-002-153
執行期間：95 年 8 月 1 日至 96 年 7 月 31 日

計畫主持人：陳文章
計畫參與人員：林佳宏、李俊賢、許麗芳、童宜峙、李文亞

成果報告類型(依經費核定清單規定繳交)：■精簡報告　□完整報告

本成果報告包括以下應繳交之附件：
□赴國外出差或研習心得報告一份
□赴大陸地區出差或研習心得報告一份
□出席國際學術會議心得報告及發表之論文各一份
□國際合作研究計畫國外研究報告書一份

處理方式：■除產學合作研究計畫、提升產業技術及人才培育研究計畫、列管計畫及下列情形者外，得立即公開查詢
□涉及專利或其他智慧財產權，□一年□二年後可公開查詢

執行單位：國立台灣大學高分子所

中　華　民　國　96　年　5 月　29 日

摘　要

嵌段共聚高分子可藉由組成比例、物理鍵結及自組裝特性而形成多重等級結構形態之超分子。本計畫除了研究不同構形之 coil-coil 嵌段共聚高分子，亦探討硬桿高分子半導體鏈段 Rod-Coil 嵌段共聚高分子之形態及光電特性。在第一年計畫已合成不同鏈段長度、比例及 arm number 之星狀(包括 blockarm 及 heteroarm)嵌段共聚高分子 poly(styrene)-*block*-poly(2-vinylpyridine)(PS-*b*-P2VP)、poly(styrene)-*block*-poly(4-vinylpyridine) (PS-*b*-P4VP)，並與 dodecylbenzenesulfonic acid (DBSA)自組裝為 structure-within-structure 之超分子結構，此結構與線性 PS-*b*-P2VP 或 PS-*b*-P4VP 做比較，而發現構形對 order-disorder transition temperature 及結構有極顯著影響。

第二年計畫之研究包括將第一年所合成的不同構形（線性 vs.星狀）PS-*b*-P4VP 在溶液下聚集行為進行探討與比較，研究發現星狀共聚物可以如線性共聚物在溶液下藉由改變溶劑環境可以得到球狀、柱狀、空心氣泡、球狀聚集及空心氣泡聚集的共聚結構；我們發現因為星狀共聚物比線性有更好的溶解性，所以星狀共聚物的聚集結構中數目會比線性低，間接說明了星狀擁有較低的聚集結構改變的趨動力。而在 Rod-Coil 嵌段共聚高分子之研究，包括製備不同分子量與組成之 polyfluorene based Rod (PF)-Coil(poly(N-isopropylacrylamide)(PNIPAA), poly(acrylic acid)(PAA), poly((ethyleneglycol methylether methacrylate)(PPEGMA), poly-(3(tripropoxysilyl) propyl methacrylate) (PPOPS) ...）硬桿-柔軟嵌段共聚高分子，並探討其在溶液或表面上特殊的結構形態與光電性質（吸收或發光）。在共聚物於表面系統的研究中（PF-*b*-PPEGMA-*b*-PPOPS），我們證明了表面結構與光電性質可以藉由溶劑環境、接枝密度及共聚物比例調控；在共聚物於溶液系統中，我們也藉由改變溶劑環境及鏈段長短得到多元聚集結構，如層狀、球狀、聚集球狀、空心氣泡狀、柱狀、反轉球狀及柱狀，在聚集結構的改變過程中，可以導致共聚物光電吸收及放射波長的明顯改變。另一個研究系統含 fluorene 側鏈之 PNIPAA 可為新穎的環境答應(pH and 溫度)功能性高分子，且其當 amino group 被離子化後，高分子因其螢光訊號隨 DNA 濃度改變而可以被利用於生物檢測系統。上述成果分別發表於 *Langmuir*, *Macromol. Rapid Commun.*(2 篇), *J. Polym. Sci. Polym. Sci.*, *Polymer*, 及 *Macromolecules*.

關鍵詞：高分子構形、活性聚合法、硬桿-柔軟嵌段共聚高分子、微結構、光電特性。

Abstract

Block copolymers could self-assemble into supramolecular materials with hierarchical morphologies through the composition、 physical bonding or hydrophobic/hydrophilic interaction. In this project, molecular architecture effects on morphology and properties of the coil-coil or rod-coil block copolymers are explored. In the first year of the proposed project, star (heteroarm or blockarm) poly(styrene)-*block*- (2-vinylpyridine) (PS-*b*-P2VP) or poly(styrene)-*block*-(4-vinylpyridine) (PS-*b*-P4VP) with various segment length, ratio or arm number were synthesized and compared with their linear analogs. Such copolymers with amphiphilic molecule dodecylbenzenesulfonic acid (DBSA) could form structure-within structure supramolecular materials. The experimental results suggested that the molecular architecture effects played an important role on the mocristructure and order-disorder transition temperature.

In the second year of the proposed project, the morphologies of different architectures (Linear vs. Hetero-arm star) PS-*b*-P4VP were characterized in dilute solution. The experimental results showed that various morphologies including spheres, cylinders, vesicles, large compound vesicles (LCVs) and large compound micelles (LCMs) were observed by varying the solvent quality arm length. Besides, hetero-arm star copolymer was found to have the lower aggregation number than linear counterparts by increasing the poor solvent quality. Fluorene based rod-coil copolymers with various coil moiety and rod-coil ratio were synthesized and characterized, including(poly(N-isopropylacrylamide)(PNIPAA), poly(acrylic acid)(PAA), poly((ethyleneglycol methylether methacrylate)(PPEGMA), poly-(3(tripropoxysilyl) propyl methacrylate) (PPOPS) .... The experimental results showed that the surface structures and photophysical properties of PPOPS polymer brushes could be manipulated by solvent quality, grafting density, and rod-coil block ratio. Various morphologies, including lamellar, spheres, large compound micelles, vesicles, cylinders, inverted spheres and cylinders, were observed by varying the coil length and the selective solvent content. Such morphological transformations resulted in the significant variations of optical absorption or fluorescence characteristics, which could be used for sensory applications. For example, fluorene containing-PNIPAA could be used as a biosensor because the fluorescence intensity varied with the DNA concentration. The above results has been published in *Langmuir*, *Macromol. Rapid Commun* .(2 papers), *J. Polym. Sci. Polym. Sci.*, *Polymer*, and *Macromolecules*.

Keywords: polymer architecture、living polymerization、Rod-coil block copolymer, morphology、optoelectronic properties

目　　錄

一、前言

精確控制高分子分子結構、形態及特性，一直是高分子科學的重要課題。嵌段共聚高分子系統可藉由組成比例、物理鍵結及自組裝特性而形成多重等級結構形態之超分子。若能賦予各層次結構不同特性、則能形成多功能智慧型材料。本研究之重要性即在於精準控制高分子系統結構自組裝形態且賦與予光電功能化特性，這對於國內高分子科學進展及高級人才培育將極有助益。

本計畫除了研究不同構形之 coil-coil 嵌段共聚高分子，亦探討硬桿高分子半導體鏈段之 Rod-Coil 嵌段共聚高分子之形態及光電特性。在第一年計畫已合成不同鏈段長度、比例及 arm number 之星狀(包括 blockarm 及 heteroarm) 嵌段共聚高分子 poly(styrene)-*block*-poly(2-vinylpyridine) (PS-*b*-P2VP)、poly(styrene)-*block*-poly(4-vinylpyridine) (PS-*b*-P4VP)，並與 dodecylbenzenesulfonic acid (DBSA)自組裝為 structure-within-structure 之超分子結構，此結構與線性 PS-*b*-P2VP 或 PS-*b*-P4VP 做比較，而發現構形對 order-disorder transition temperature 及結構有極顯著影響。本子計畫第二年有兩個研究目標，首先為將第一年所合成的不同構形 PS-*b*-P4VP 在溶液下聚集行為進行探討與比較；另一個目標則導入硬桿共軛高分子鏈段到共聚物系統，並以活性聚合法製備不同分子量與組成之 polyfluorene based Rod (PF)- Coil（PNIPAA, PAA, PPEGMA, PPOPS ...）硬桿-柔軟嵌段共聚高分子，且探討其在溶液或表面上特殊的結構形態與光電性質（吸收或發光）。

二、研究目的

(1) Molecular architecture effects on the morphologies of PS-b-P4VP:

探討溶液品質對不同構形 PS-*b*-P4VP 之溶液聚集行為影響；固態結構特性則由陳信龍教授計畫研究。

(2)Synthesis, morphologies and photophysical properties of rod-coil block copolymers: 探討不同柔軟鏈段特性、鏈段長度、硬桿柔軟鏈段比例對 fluorene 嵌段共聚物之聚集形態及對光電性質之影響且探討其環境應答應用。

三、研究方法與原因

本計畫採用之研究方法與原因，如下表所述:

研究原因	研究方法
目前文獻中缺乏星狀與線性嵌段共聚高分子 PS-*b*-P4VP 在溶液下聚集行為的比較與探討	以不同構形 PS-*b*-P4VP 嵌段共聚物在混合溶液下使其聚集，並利用 TEM, SLS, DLS 進行聚集行為的探討與比較。
目前文獻中缺乏 rod-coil 嵌段性共聚高分子於溶液或表面聚集形態之研究及其相關應用。	結合功能性共軛高分子及活性聚合法製備不同分子量與組成之 polyfluorene based Rod (PF)- Coil（PNIPAA, PAA, PPEGMA, PPOPS ...）硬桿-柔軟嵌段共聚高分子，並探討其在溶液或表面上特殊的結構形態與光電性質（吸收或發光）之關係及其環境應答應用。

四、研究成果與討論

1. Architecture effects on the Morphologies of PS-b-P4VP in dilute solutions

In this study, hetero-arm star polystyrene-b-poly(4vinylpryridine) (PS_n-$P4VP_n$) and linear counterparts were synthesized by sequential anionic polymerization and their morphologies in dilute solutions were studied. Although micellization of star-shape copolymers has been intensively studied in different selective solvent, aggregated behavior and related morphological transition in mixed solvent are rarely explored. In this study, multiple morphologies of heteroarm star PS_n-$P4VP_n$ were observed by varying solvent quality and compared with their linear with analogs. Two different arm numbers of PS_n-$P4VP_n$ with similar composition and degree of polymerization were synthesized to explore the architecture effects. The morphologies of copolymers were investigated by TEM and dynamic and static light scattering in dilute solutions of water and DMF mixtures. Note that DMF is common solvent for both blocks and water is selective solvent for the P4VP blocks as pH is below 5.0. The experimental results suggested the importance of polymer architecture on the micellar morphologies in dilute solutions.

1-1 Experimental

Material

The block copolymers used in this report were synthesized by the sequential anionic living polymerization. Solvent and monomers required in the reaction are purified before synthesis. The reaction was carried out at -78℃. In the first, the PS precursors were prepared by using sec-Butyllithium (*sec*-BuLi) as initiator, and then second monomer, 4-vinylpyridine (4VP), was added to the reaction to polymerize the diblock copolymers. However, synthesis of hetero-arm star PS_n-$P4VP_n$ has additional step before adding 4VP (**Figure 1-1**). Small amount of divinyl-benzene (DVB) was introduced after completely consumption of styrene. In this step a living PS_n star copolymers were obtained by bearing a number of active sites within its cores. Then, P4VP can be grown from cores after adding 4VP to the reaction mixture. Finally, the reaction was deactivated by methanol, precipitated in hexane, and then filtered out to obtain the product.(**Table 1-1**)

Sample Preparation

Sample solutions of PS-b-P4VP were prepared by first dissolving the copolymers in N, N-dimethylformamide (DMF) which is common solvent for both blocks, with an initial polymer

concentration of 2.0 mg/ml. The solutions were kept stirring overnight to make homogeneous state. Then, a given weight of deionied water, a selective solvent for P4VP as pH is below 5.0 but a poor solvent for PS, was dropped gradually into to the copolymer/DMF mixtures under moderate mechanical stirring. The solutions were kept stirring for 3 days to reach equilibrium morphologies before characterization. The samples we selected in the system are heteroarm star **PS_4-$P4VP_4$** (Mn=97900, Mw/Mn=1.17, f_{4vp}=0.24), which average arm numbers are 8.3 and the compositions of the blocks are signed by f_{4vp} which is molar ratio of 4-vinyl pyridine per star copolymer.

1-2 Results and Discussion

Morphological Transformation Induced by Adding Selective Solvent

The morphologies of micelles are examined under TEM after removing the residual solvents completely. **Figure 1-2** shows a series of TEM images of the micellar morphologies for solution varying water content. The aggregates are spherical at water concentration of 5.7 wt% (**Figure 1-2A**). Besides, the diameter of the spheres is nearly about 45 nm. Note that the values of the hydrodynamic diameter of the micellar aggregates detected by DLS are a little larger than those observed by TEM. It is because the micelles are swollen in solution, while TEM observation shows the diameter of the aggregates deposited onto to a copper grid and dried under vacuum. As a water concentration at 8.3 wt%, cylinder morphology is shown and mixed with spherical micelles (**Figure 1-2B**). On further increasing the water content to 10.9 wt%, mixed cylinders and vesicles appear are exhibited(**Figure 1-2C**). Furthermore, **Figure 1-2D** shows the predominant vesicle structures at water content of 13.5 wt%. Finally, the morphology changes to large compound vesicles (LCVs) at water content of 16.1 wt% (**Figure 1-2E**). If water is added further, the morphology does not change continuously.

The above morphology results can be explained as below. As the solvent quality becomes progressively poor for the core-forming block with increasing selective solvent, the aggregates may change its morphology due to energy constraint. It can be explained that poor solvent quality would increase interfacial tension, leading to raise the interfacial energy. In response to this increase, the system tends to decrease the total interfacial area by increasing the micellar radius. However, in the process of the core enlargement, the stretching of polymer chains in the core increases and results in an increase of free energy. When the stretching energy predominate the total free energy, an

aggregate has to adapt another geometry to relax the stretching, whereby the interfacial area is smaller and core-chain stretching is reduced. In another words, as the morphology changes from spheres to cylinders, to vesicles, both values of the degree of stretching for core blocks and interfacial area per chain reduce. Hence, we observe the above morphological transformation induced by varying water content. The DLS results also reveal the tendency of increasing micellar radius with adding water content.

LCVs in **Figure 1-2E** are of special interest for the application of drug delivery. The TEM images show the uniformity and the equality of the thickness of both inside and outside walls of the compound vesicles. It is assumed that LCVs may be formed from undergoing secondary aggregation of individual vesicles. It indicates that the individual vesicles formed first and then associated into large compound vesicles in order to minimizing surface free energy, called kinetic controlled morphology. Consequently, morphological transformation can also be turned from spheres to cylinders, and then to vesicles for star-shape copolymers and the aggregated morphology transition mechanism proposed is illustrated in **Figure 1-3**.

Architecture Effect on Morphological Transformation

Linear **PS-*b*-P4VP** was also prepared in our study in order to investigate architecture effect on micellar behavior by keeping the compositions of linear and star copolymers similar and having nearly the same block length as those of the star arms (L1 vs.H2). It has been found previously that size growth of micelles is the driving force of morphological transition due to energy concepts. The representative plot for the hydrodynamic diameter (D_h) determination is illustrated in **Figure 1-4**, which is investigated by DLS again. According to the results, critical water contents for micellization of two copolymers are located between 2.8 and 5.7 wt% on account of D_h increasing sharply from the unimers. In addition, the D_h of L1 is a little larger than H2 for whole points and having 1.4 times of slope to H2 for R_h as a function of water content. From the literatures, Tsitsilianis et al. had published that the R_h dependence for heteroarm star **PS_6-$P2VP_6$** in toluene, good solvent for PS, can be presented as $R_h \sim N_{agg}^{1/3} N_{P2VP}^{1/3}$, where N_{agg} and N_{P2VP} denote aggregation number of polymer chains within micelles and repeat units of **P2VP** of block copolymers, respectively. Other examples published by Foster as well shown a scaling relation $R_h \sim N_{agg}^{1/4} N_{P4VP}^{1/2}$ for linear **PS-*b*-P4VP** in toluene. There are numerous examples to illustrate similar

relationship. It is appropriate to express that the R_h of micelles increases with raising the aggregation number and the length of the insoluble arms. We believe that the dependence of R_h on two factors of the examples can be used and discussed analogously in our study because of similar molecular structures and architectures. On further simplification, the domain size can then be scaled as $R_h \sim N_{agg}^{x}$ where $x > 0$ due to owning virtually block length in our system for a pair of copolymers. Interestingly, we founded L1 has higher N_{agg} and greater tendency of raising N_{agg} with increasing water content than H2. To better understand these findings, **Figure 1-4** shows the changes in N_{agg}, with increasing water content, estimate by SLS. It should be noticed that N_{agg} of H2 at results was multiplied by 4.15 since each star copolymer comprises 8.3 PS and P4VP chains. The results indicate that number of chains in the aggregates for L1 or H2 is increased with depressing solvent quality. Nevertheless, N_{agg} of H2 has lower numbers and lower favorable to increase with adding water compared with L1. For example, N_{agg} of L1 and H2 are 452 and 265 at 8.3 wt% and then increased to 673 and 429 at 10.9, respectively. This observation is in agreement with DLS and lead to imply effect of architecture in solution micelles.

From the concepts of morphological transition we mentioned previously, the tendency of increasing N_{agg} and R_h was the driving force for transformation. It seems that heteroarm star PS_n-$P4VP_n$ has lower motivation for the phenomena of multiple morphologies due to architecture effect. It had been published heteroarm star **PS_6-$P2VP_6$** had higher free energy of micellization, implying a lower driving force for micellization, which was caused to a loss of combinatorial entropy as the polymer chains attached to the core in the micellar form compared with free chains. To put the matter simply, the heteroarm star copolymers can protect their insoluble blocks more easily than the corresponding linear copolymers. Since adding water content can induce micellization and morphological transition by enlarging size of aggregates, it seems heteroarm star copolymers have higher toleration of selective solvent. Therefore, the results lead us to the conclusion that lower driving force of morphological transition for heteroarm star copolymers compared with linear counterparts due to better solubility for former. Combined with the TEM observations, L1 can obtain vesicle morphology earlier than H2 (10.5 wt%) at water content of 8.6 wt%.

1-4 Conclusions

Variation of micellar morphology of hetero-arm PS_4-$P4VP_4$ in different solvent quality was investigated. Various morphologies including spheres, cylinders, vesicles and large compound vesicles (LCVs) were observed when the poor solvent of water for the PS blocks was increased. Large compound micelles (LCMs) were also observed in the shortest soluble block length. For micelles the R_h and the tendency of raising R_h with adding water were both found to be larger in the case of the heteroarm star copolymers than those of linear analogs by DLS. SLS results further verify the relationships between N_{agg} and solvent quality in two kinds of architectures. The experimental results suggest that molecular architecture effect plays an important factor on micellar morphologies.

2. Synthesis and Characterization of rod-coil PF-*b*-PPEGMA-*b*-PPOPS copolymers

In this study, a joint theoretical and experimental investigation of conjugated rod-coil block copolymer brushes is reported. The theoretical analysis of the rod-coil block copolymer brushes by DPD was seldom explored. The effects of solvent stimuli and grafting density of polymer brushes on the surface structures by DPD were investigated. The multifunctional amphiphilic triblock copolymer, poly-[2,7-(9,9-di-n-hexylfluorene)]-b-poly-[poly(ethylene glycol) methyl ether methacrylate]-b-poly-[3-(tripropoxysilyl)propyl methacrylate] **(PF-b-PPEGMA-b-PPOPS)**, were synthesized. The block copolymers were assembled onto a glass substrate with the silanol groups of **PPOPS** blocks anchored on the surface. The surface structures and photophysical properties of the polymer brushes were investigated. The present study demonstrates how the surface structures and photophysical properties of rod-coil block copolymer brushes response to environmental stimuli.

2-1 Theoretical Methodology

The polymer model and simulation based on dissipative particle dynamics (DPD).[3] are described as follows. In our system (volume $V = L_x \times L_y \times L_z = 30 \times 30 \times 20$ with N particles, and the total number density $\rho = N/V = 3$), the polymer brush is modeled as a copolymer with sections of rod and coil blocks. The end-beads of the coil blocks are attached to an impenetrable surface at z =0. The lengths of the rod and coil blocks are represented by n_A and n_B, and fixed at 5 and 20 (i.e. n_A=5, n_B=20), respectively. The total number of particles in the system is $N = N_S + N_P(n_A + n_B)$, where N_S

and N_P are the numbers of solvent particles and polymer brushes. We define *grafting (surface) density* $\rho_S = N_P/(L_x \times L_y)$. The effect of different degrees of grafting on the surface structures is also studied and the grafting density (ρ_S) spans from 0.1 to 1.0. Like MD, the DPD particles obey Newton's equation of motion. In addition to the three different pairwise-additive forces (conservative, dissipative and random forces) considered in DPD simulations, the spring force ($\mathbf{F}^S$) and angle force ($\mathbf{F}^\theta$) describing the chemical bonding and angle bending effects of the polymer chain are also taken into account in this system and are

$$\boldsymbol{F}_{ij}^{S} = c(\mathbf{r}_{ij} - 0.7)$$

$$\boldsymbol{F}_{ij}^{\theta} = \begin{cases} k_\theta(\theta - \pi)^2 & \text{(for rod)} \\ 0 & \text{(for coil)} \end{cases}$$

In this work, we have chosen c = 100 and k_θ = 20.

Groot and Warren showed that the repulsion parameter (a_{ij}) of 25 corresponds to a highly compatible pair. As the repulsion parameter increases, the compatibility between *i* and *j* particles decreases. In our study, a_{AS}, a_{BS}, and a_{AB}, represent the maximum repulsive forces between rod block and solvent particle, coil block and solvent particle, and rod and coil blocks, respectively. We chose a_{AS} = 26 to symbolize the solvophilic nature of the rod block and a_{AS}=40 to denote the solvophobic character of the rod block. The a_{BS} and a_{AB} were set to be 26 and 40, respectively, indicating good solvent condition for the coil block and incompatible characteristics between rod and coil blocks.

2-2 Experimental

Material

All of the reagents were purchased from Aldrich and used as received except for Poly(ethylene glycol) methyl ether methacrylate (PEGMA, Mn ≈ 300), which was distilled under vacuum. 3-(Tripropoxysilyl)propyl methacrylate (POPS), 2,7-dibromo-9,9-di-n-hexylfluorene (**1**), and 2-bromo-9,9-di-n-hexylfluoreneboronic acid (**2)** were prepared according to known procedures.

Polymer Synthesis

Polyfluorene macroinitiator, α-{4-[2-(2-bromo-2-methyl-propoyloxy) -methyl] phenyl} -ω-bromo-poly[2,7-(9,9-dihexylfluorene)] (**4**), was synthesized as described below: First, α-[4-(2-Hydroxylethyl)phenyl] -ω-bromo-2,7- (9,9-dihexylfluorene) **(3)** was synthesized according to the literature. Then, it was reacted with 2-bromoisobutyryl bromide to obtain the **4**. The amphiphilic triblock copolymers of **PF-*b*-PPEGMA-*b*-PPOPS** were prepared by atom transfer radical polymerization (ATRP), as shown in **Figure 2-1**.

Self-Assembly of Triblock Copolymers on Oxidized Surfaces and Solvent Stimuli

The polymer brushes were prepared by using a new surface-reactive method developed by Thomas et al. In order to investigate the responses corresponding to environmental stimuli, the polymer brushes were immersed into either toluene (good solvent of both the **PPEGMA** block and the **PF** block) or methanol (good solvent of **PPEGMA** block but non-solvent for **PF** block) for 30 minutes at room temperature and then dried under a flow of clean air before characterization.

2-3 Results and Discussion

Theoretical Investigation on the Surface Structures of Rod-Coil Block Copolymer Brushes

Figure 2-2 represents the surface structures of rod-coil block copolymer brushes in the good solvent and poor solvent for rod blocks. The yellow and red spheres correspond to the particles in the rod and coil blocks, respectively. The blue spheres are the anchoring points of the rod-coil copolymers on the surface. For the polymer brushes immersed in common solvent (**Figure 2-2(a)**), the rod blocks are well-dispersed on the surface due to the good compatibility between the rod blocks and the solvents. However, aggregative domains of the rod blocks are observed in **Figure 2-2(b)**. The incompatibility between the rod blocks and the solvent particles drives the rod blocks into forming aggregates to reduce the contacts between rod blocks and solvents.

Figure 2-3 shows the surface structures of the rod-coil block copolymer brushes with grafting density of 0.1~0.9 in the poor solvent for the rod blocks. The surface structures show no distinguished variation with different grafting densities if the polymer brushes are in the good solvents for both the rod and coil blocks. The only difference is the surface coverage. Nevertheless, the surface structures are greatly affected by the grafting density if the polymer brushes are

immersed in the poor solvents for the rod blocks. The rod blocks forms a series of small isolated islands on the surface when the grafting density is as small as ρ_S = 0.1, as shown in **Figure 2-3(a)**. The size of these isolated islands increases with increasing grafting density (ρ_S = 0.5). Then, worm-like conformation is revealed from the interconnection of these isolated islands as the grafting density increases to 0.7 **(Figure 2-3(c))**. Finally, the worms begin to intertwine and network-like surface structures disclose (ρ_S =0.9).

Experimental Results of PF-b-PPEGMA-b-PPOPS Rod-Coil Block Copolymer Brushes

The polymer brushes are named as **PB1**, **PB2**, and **PB3** corresponding to the concentration of polymer solution equals to 20, 10, and 5 mg/mL, respectively. Representative AFM images of polymer brushes **PB1~PB3** are given in **Figure 2-4**. **Figures 2-4(a)** is the height image of the polymer brush **PB1** after the toluene treatment. The surface is relatively smooth; the roughness is 1.45 nm. **Figures 2-4(b)** is the height image of the polymer brush **PB1** after the methanol treatment. The surface becomes relatively rough with a roughness of 6.97 nm. Note that methanol is a good solvent for **PPEGMA** block but a poor solvent for **PF** block. The **PPEGMA** blocks are swollen with methanol resulting in its moving up to surface. Whereas, the **PF** blocks are possibly covered by the PPEGMA resulting in its falling down to the substrate. Both effects lead to opposite movement of the blocks and hence, aggregated islands of **PF** blocks with large dimension and even interconnected, worm-like structures are formed. **Figures 2-4(c)** and **2-4(d)** are the height images of the polymer brushes **PB2** and **PB3** after the methanol treatment, respectively. The surface roughness of **PB2** and **PB3** is 5.63 and 0.75 nm, respectively. It can be seen that the size of the aggregated domains of **PF** blocks increases with increasing grafting density. Finally, some interconnected worm-like structures are formed on the surface of polymer brush **PB1**. The variation of surface structure with grafting density is exactly the same as the theoretical prediction as shown in **Figure 2-3**.

Figure 2-5 represents the photoluminescence (PL) spectra of polymer brushes after toluene and methanol treatment excited at the wavelength of 380 nm. All the polymer brushes after toluene treatment show typical emission peaks of polyfluorene. After methanol treatment, additional emission shoulders around 475-488 nm were observed. Furthermore, this additional shoulder shows increasing intensity with increasing grafting density. Such a result clearly indicates that the **PF**

blocks aggregate and possibly to form excimers in the polymer brushes.[9] Therefore, the fluorescence results are in good accordance with the AFM studies as described above.

2-4 Conclusions

The simulated surface structures by DPD method showed that the aggregation of the rod blocks was triggered by their poor solvents and the conformation of the aggregation was affected by the grafting density of the polymer brushes. For the justification of our theoretical model, a new rod-coil block copolymer, **PF-*b*-PPEGMA-*b*-PPOPS**, and its corresponding polymer brushes were synthesized by the grafting-to method. The experimentally observed surface effects of solvent stimuli and grafting density on the surface structure were in a good agreement with the theoretical results. The photophysical characteristics of the polymer brushes were also in consistence with their surface structures. The present study demonstrates that the surface structures and photophysical properties of rod-coil block polymer brushes could be manipulated by solvent quality and grafting densities.

3. Synthesis and Characterization of rod-coil PF-PAA copolymers

In this study, synthesis, morphology, and photophysical properties of rod-coil block copolymers poly[2,7-(9,9-dihexylfluorene)]-*block*-poly(acrylic acid) (**PF-*b*-PAA**) with three different coil lengths are reported. The chemical structures of the studied polymers are shown in **Figure 3-1**. The morphologies of **PF-*b*-PAA** were investigated in different mixed solvents and correlated with the coil length and the selective solvent content. It is first time to observe fluorene-based rod-coil block copolymers with various morphologies of lamellar, sphere, large compound micelle, cylinder, and vesicle, etc, in dilute solution as far as we know. Moreover, the optical absorption and photoluminescence properties of the **PF-*b*-PAA** were used to understand the aggregation-induced π–π stacking in dilute solution.

3-1 Experimental

Materials

Polyfluorene macroinitiator, (**PF-Br**), was synthesized according to the literature. Then, (PF-*b*-PtBA) and PF-*b*-PTMSPMA was synthesized from PF-Br by atom transfer radical polymerization. The *tert*-butyl esters of **PF-*b*-PtBA** were cleaved via reaction with trifluoroacetic

acid (TFA) in dichloromethane, giving the **PF-*b*-PAA**. The studied solutions were prepared by dissolving the polymer in common solvent and then selective solvent was added with the proper volume ratios in which the polymer concentration was maintained at 0.1-0.2 wt % in solution.

Morphology Characterization of Polymer Aggregates in Solution

The aggregate morphology was characterized by TEM using JEOL 1210 operating at an acceleration voltage of 100 kV. A drop of the aggregates dispersion was cast onto a 200-mesh copper TEM grid deposited by carbon and dried in vacuum for TEM images.

3-2 Results and Discussion

Self-assembly of PF-b-PAA

Figure 3-2(a)-(c) show representative TEM images of the micellar structures derived from the **PF_7-*b*-PAA_{26}** in DCM/methanol mixed solvent with methanol contents of 10, 25, and 50 vol%, respectively. Since the methanol is a poor solvent for **PF,** the rod **PF** chains packed as long strips to minimize the interfacial energy between the rod block and methanol. Such structures could be resulted from the PF lamellar domains between solvated **PAA** chains. While the **PF** aggregated domains favor ordered packing with their long axes aligned, the corona PAA chains are too short to change the chain conformations by varying methanol contents. Thus, no significant changes in morphologies of **PF_7-*b*-PAA_{26}** were observed with increasing methanol contents. PF_7-b-PAA_{50} in a DCM/methanol mixed solvent with methanol volume contents of 10, 25, and 50%, exhibit coexisting structures of spherical and large compound micelles (LCMs), spherical and vesicle morphology as shown in **Figure 3-2 (d)-(f)**. As the methanol content increases, it enhances the degree of swelling between methanol and **PAA** and the interfacial tension between the PF core and **PAA** corona. Thus, micelle shape changes, which is similar to the packing factor mechanism proposed in the literature.

As the **PAA** coil length increased further, an interesting phase inverse morphology occurred even at a low methanol content solvent. **Figure 3-3 (a) and (b)** show the spherical and cylinderical structures **PF_7-*b*-PAA_{70}** in DCM/methanol solution with the methanol content of 10 and 25 vol%, , respectively, in which a bright core of **PAA** block surrounded by a dark corona of **PF** block. The morphology transition from spherical of **Figure 3-3(a)** to cylinder of **Figure 3-3(b)** is probably

because the swelling of the inner **PAA** core is enhanced with increasing methanol content and leads to an increased interfacial area for cylinder formation. As the methanol content is further increased to more than 25 vol% of **Figure 3-3 (c) to 3-3(e)**, the solubility of **PAA** chains is enhanced and results in aggregates with the **PAA** corona and the PF inner core. In addition, a significant morphology transformation from inverted cylinder to spherical vesicles and eventually nanorods with increasing methanol content is observed in Figure **3-3(c)-3-3(e)**. The nanorods with dark core and bright corona are contrary to the inverted cylinder shown in **Figure 3-3(b)**. The cylindrical structure of these micelles in Figure **3-3(d)-3-3(e)** might be partly explained by the more cone-shaped conformation of the long chain-based rod-coil molecules and a second driving force might be strong $\pi-\pi$ interactions among aromatic segments down the long axis of the rods. The morphological transformation of the **PF_7-*b*-PAA_{50}** and **PF_7-*b*-PAA_{70}** driven by the selective solvent are summarized in **Figure 3-4.**

Photophysical Properties

Figure 3-5 shows the optical absorption spectra and photoluminescence (PL) spectra of **PF_7-*b*-PAA_{70}** in dilute solution of DCM and methanol with methanol contents ranging from 0 to 90 vol%. The absorption peak maximum due to the $\pi-\pi^*$ transition of the **PF** block shifts from 374 to 350 nm as the methanol content increased from 0 to 90 vol%. This blue shift suggests the reduction of the effective conjugated lengths since the PF block becomes more non-planar on account of the aggregates formation by its poor solvent of methanol. It could be explained by the molecular exciton model, assuming H-type aggregation formed by a parallel orientation of **PF** segments. The photoluminescence spectra of the aggregates also exhibited dramatic changes, as shown in **Figure 3-5**. There are two major emissions at 415 and 435 nm for the **PF_7-*b*-PAA_{70}** in pure DCM solution. As the methanol content increased to 90 vol%, the emission peak at 415 nm is blue-shifted to 407 nm while that at 435 nm shifted to 426 nm. Such peak shifting is a consequence of interchain $\pi-\pi$ interaction between parallel **PF** blocks resulted from aggregation and accompanied by strong fluorescence quenching with the quantum efficiency (ϕ_f) decreased from 0.88 to 0.27 (see insert of **Figure 3-5(b)**). The ϕ_f decreased with increasing the methanol content further indicates the H-type aggregation formation of the **PF** block.

3-3 Conclusions

Morphologies and photophysical properties of three amphiphilic rod-coil diblock copolymers of **PF-b-PAA** with different coil lengths have been studied. Various morphologies, including lamellar, spheres, large compound micelles, vesicles, cylinders, and inverted spheres and cylinders, are observed by varying the coil length and the selective solvent content. Such morphological transformations could induce the significant variations of optical absorption or fluorescence characteristics because of possible H-aggregation formation. The present study suggests the significance of the rod/coil ratio and selective solvent content on the aggregate morphologies and photophysical properties of the rod-coil block copolymers.

4. New Environmentally Responsive Fluorescent PNIPAA Copolymer for DNA Sensing

Here we report the synthesis and investigation of a **PNIPAA** copolymer with functional fluorene moieties. A new fluorene dimer as the monomer (M), depicted in **Figure 4-1** with ternary amino groups, was deigned and synthesized first. This material provides sensitivity to the pH value because of the amine group and can be further quaternized to accommodate a sensing ability for DNA molecules. This is the first time that a functional pHsensitive fluorene-containing polymer has been integrated with temperature-responsive **PNIPAA** to the best of our knowledge. The intelligent material reported here has been demonstrated to have pH-, temperature-, and DNA-sensing ability through ultraviolet–visible (UV–vis) absorption and fluorescence measurements in aqueous solutions.

4-1 Experimental

Materials

All commercial reagents were purchased from Aldrich and used as received. The purification of all the solvents was followed by a common distillation procedure. All reactions were conducted with oven-dried glassware under a nitrogen atmosphere and were stirred magnetically. The plasmid DNA molecule (bp =9931) used in demonstrating the responsive property of the quaternized NIPAA copolymers was obtained by the standard extraction procedure. The Briton–Robinson buffer was used in this study. The synthetic scheme of the monomer and copolymers are shown in **Figure 4-1** and **Figure 4-2**, respectively.

4-2 Results and Discussion

Figure 4-3 shows the UV–vis absorption and fluorescence emission spectra of the copolymers, **P1** and **P2**, in aqueous solutions. The Peak wavelength (kmax) on the absorption spectrum of **P2** (347 nm) that arose from the fluorene moiety has a 12-nm redshift in comparison with that of **P1** (335 nm). The fluorescence spectra of **P1** and **P2** are also quite different. **P2** shows a sky blue emission at kmax =460 nm with a low quantum yield of 0.18, whereas **P1** has a pure blue emission at 390 nm with a high quantum yield of 0.77. These results suggest a significant variation in the photophysical properties by the quaternization of the amine in the fluorene moiety. The more rigid chain conformation of the **P2** electrolyte, compared with that of the neutral precursor **P1**, might be used to explain these results, which are similar to those of conjugated fluorene-based polyelectrolytes reported in the literature. The LCST characteristics of **P1** were examined by the variation of the optical transmittance spectra with the temperature. **Figure 4-4** shows the optical transmittance of **P1** in an aqueous solution at 550 nm heated from room temperature to 40°C. The transmittance slope changes dramatically around 31.5 8C, which is very close to the LCST (32°C) of pristine **PNIPAA** polymers. This suggests that the incorporation of the fluorescent moiety into the polymers does not change the hydrophobicity/hydrophilicity significantly near the **PNIPAA** polymer main chain.

Figure 4-5 shows the fluorescence emission spectra of **P1** in water solutions with different pH values ranging from 5 to 11. In each pH buffer solution, the temperature-controlled spectra were collected from 22 to 40°C. As pH =7, the fluorescent spectra show a similar fluorene feature, which is invariant with the pH and temperature, as demonstrated by the typical example of pH 5 in **Figure 4-5(a)**. However, at pH > 7, a broad and featureless aggregation emission appears below 32 .°C and results in the redshift of the emission spectra, as demonstrated by the typical example of pH=9 in **Figure 4-5(b)**. These broad and featureless aggregations dissociated when the solutions were heated to 40.8°C, and the fluorene features appear in spectrum 6 of **Figure 4-5(b)**. **Figure 4-5(c)** exhibits the variation of the normalized fluorescence intensity (IT/I10 8C, where IT is the fluorescence intensity at temperature T and I108C is the fluorescence intensity at 10°C) at 388 nm at pH values of 5, 7, and 9 and at temperatures ranging from 22 to 40°C. It shows that the emission intensity of P1 at a basic condition of pH 9 is significantly enhanced when the temperature is higher than 32 °C, which suggest the important role of the LCST transition. **Figure 4-6** illustrates a possible

mechanism for the behaviors of **P1** in water. For the acidic condition, the fluorene segments are slightly protonized because of the ionized hydrogen. The slightly protonized fluorene segment improves its solubility in a water solution, and thus the featured fluorine spectrum is shown in **Figure 4-5(a)**. On the other hand, under the basic condition, the fluorine segments aggregate at room temperature even in water-soluble **PNIPAA** because of the poor solubility of the fluorene moiety in water. When the temperature is higher than the LCST, the microenvironmental polarity near the main chain of **PNIPAA** decreases considerably. Because the fluorene moiety favors the nonpolar environment, the decreasing polarity near the main chain improves the solubility of the fluorine segments to dissociate the aggregation, and the featured fluorene spectrum can be observed. The dissociation of the aggregations around the LCST of **P1** demonstrates that the LCST property has a significant impact on the photophysical properties of the copolymer.

Figure 4-7 shows the fluorescence emission spectra of **P2** in aqueous solutions at pH 9. **P2** shows a single, broad emission peak around 453 nm, and the maximum intensity was slightly enhanced as the temperature was increased from 22 to 40 8C; this is quite different from that of P1, which is shown in **Figure 4-5(b)**. The fluorescence spectra of **P2** at pHs 5 and 7 also show insignificant variation with the temperature. This suggests that the LCST property of **P2** does not influence the fluorescence characteristic in the studied pH range. A possible explanation for this result is that the quaternized fluorene dimer in **P2** shows a more rigid backbone than that of **P1** and such a backbone could not be further varied with the temperature in an aqueous solution. The inset of **Figure 4-7** shows the variation of the optical transmittance of **P2** with the temperature. The transmittance temperature curve slope suggests that **P2** has an LCST around 31.7 ℃. Although **P2** is not sensitive to fluorescence, the LCST characteristic is similar to that of **P1**. The DNA-sensing characteristic of **P2** was tested with plasmid DNA. **Figure 4-8** shows a substantial decrease in the emission intensity of P upon the addition of the DNA. The interaction between cationic **P2** and secondary and tertiary DNA forms a specific complex structure and results in fluorescence quenching.

Possible mechanisms for the quenching emission include the relaxation or contraction of this complex structure, the self-quenching of the aggregation of multiple units near the negatively charged plasmid DNA molecules, and the photoinduced charge transfer from **P2** to the DNA base.

The results demonstrate the sensing ability of the water-soluble, fluorene-containing copolymers, although the fluorine moiety is just a dimer. This result may provide important information for the further design of the functional polymer for DNA sensors.

4-3. Conclusions

A novel multifunctional polymer (**P1**) showing both pH and temperature sensitivity was successfully synthesized through the copolymerization of NIPAA with a new monomer having a fluorine dimer as the side group. The protonation of the amino groups on the fluorene moiety under an acidic condition improved its solubility in water. Thus, no aggregation of the fluorene moiety was observed, and the fluorescence property of **P1** was not affected by the LCST transition. However, polymer chain aggregation occurred under the basic condition because of the hydrophobic characteristic of the fluorene moiety and resulted in fluorescence quenching. Such aggregation could be resolved at a high temperature above LCST. This study may provide a new methodology for the molecular design of new environmentally (pH and temperature) stimulated functional polymers. Furthermore, after the amino groups were quaternized, the obtained polymer (**P2**) could be used as a biosensor because the fluorescence intensity
varied with the DNA concentration.

五.參考文獻 (選列)

1. Surin, M.; Marsitzky, D.; Grimsdale, A. C.; Müllen, K.; Lazzaroni, R.; Leclère,P.; *Adv. Funct. Mater.* **2004**, *14*, 708.
2. Park, J. W.; Thomas, E. L. *J. Am. Chem. Soc.* **2002**, *124*, 514.
3. Weinfurtner, K. H.; Fujikawa, H.; Tokito, S.; Taga, Y. *Appl. Phys. Lett.* **2000**, 76, 2502.
4.Antonietti, M.; Förster, S. *Adv. Mater.* **2003**, *15*, 6243.
5.Hoeben, F. J. M.; Jonkhijm, P.; Meijer, E. W.; Schenning, A. P. H. J. *Chem. Rev.* **2005**, *105*, 1491.
6.Wang, D.; Moses, D.; Bazan, G. C.; Heeger, A. J.; Lal, J. *J Macromol Sci Pure Appl Chem.* **2001**, 38, 1175–1189.
7. Huang, F.; Hou, L.; Shen, H.; Yang, R.; Hou, Q.; Cao, Y. *J .Polym Sci Part A: Polym Chem*, **2006**, 44, 2521–2532.
8. Uchiyam, S.; Matsumura, Y.; de Silva, A. P.; Iwai, K. *Anal Chem*, **2003**, 75, 5926–5935.
9. Bronich, T. K.; Nguyen, H. K.; Eisenberg, A.; Kabanov, A. V. *J. Am. Chem. Soc.* **2000**, 122,

8339–8343.

10. Groger, S.; Geschke, D.; Karger, J.; Stallmach, F.; Konak, C. *Macromolecular Rapid Communications* **2004,** 25, (10), 1015-1018.

11. Bhargava, P.; Tu, Y.; Zheng, J. X.; Xiong, H.; Quirk, R. P.; Cheng, S. Z. D. *Journal of the American Chemical Society*, **2007**, 129, (5), 1113-1121.

六. 計劃結果及自評

由上述之結果可知，本研究團隊已順利完成第二年之研究計畫，即可藉由改變溶液環境得到多元的高分子共聚結構，光電性質也隨之呈現不同的變化。未來第三年計劃將繼續對硬桿柔軟系統做更深入研究。並嘗試合成不同構形如星狀、梳狀或 Y 型的硬桿柔軟嵌段共聚物，以探討高分子構形對共聚物之聚集行為及光電性質的影響。

七. 本年度(2006//1~2007/7/31)經由本計畫經費支持所發表期刊論文目錄: (見附錄)

1. Tung, Y. C.; Wu, W. C. ; Chen, W. C.*; *Macromol. Rapid. Commun.* **2006**, *27*, 1838.

2. Yang, C. C.; Tian, Y. C. ; Jen, Alex K.-Y.*; Chen, W. C.*; *J. Polym. Sci. Part. A: Polym. Chem.* **2006**, 5495.

3. C. C. Yang, Y. Tian, C. Y. Chen, Alex K.-Y. Jen* and W. C. Chen*, "A Novel Benzoxazole-containing Poly(*N*-isopropylacrylamide) Copolymer as Multifunctional Sensing Materials", *Macromol. Rapid Commun.* 2007, 28, 894-899.

4. 6. H. L. Chen,* J. S. Lu, C. H. Yu, C. L. Yeh, U. S. Jeng, W. C. Chen, "Tetragonally Packed Cylinder Structure via Hierarchical Assembly of Comb-Coil Diblock Copolymer", *Macromolecules* 2007, 40, 3271-3276(2007).

5. Wu, W. C.; Tian, Y. C. ; Chen, C. Y.; Lee, C. S.; Sheng, Y. J.; Chen, W. C.*; Jen, Alex K.-Y.*; *Langmuir* **2007**, *23*, 2805.

6. C. H. Lee, W. C. Chen,* J. Y. Hsu, and H. L. Chen*, " Effect of Molecular Architecture of Copolymer Template on the Morphology of Mesoporous Methylsilsesquioxane", *Polymer* **2007**, in press.

八、附表及圖

Table 1-1. Characterization data of PS-b-P4VP (L1) and PS_4-$P4VP_4$ (H1~H4) block copolymers

Sample[a]	**Mw**[b] overall	**Mw**[c] PS-arm	**Mw**[d] P4VP-arm	**Mw/Mn**	**N**[e]	$\mathbf{f_{P4VP}}$[f]
H1	122200	18200	10900	1.18	8.1	0.37
H2	97900	18100	5800	1.17	8.3	0.24
H3	90100	18600	2600	1.18	8.0	0.12
H4	85300	18000	1400	1.10	8.1	0.07
L1	21900	17500	5500	1.06	-	0.24

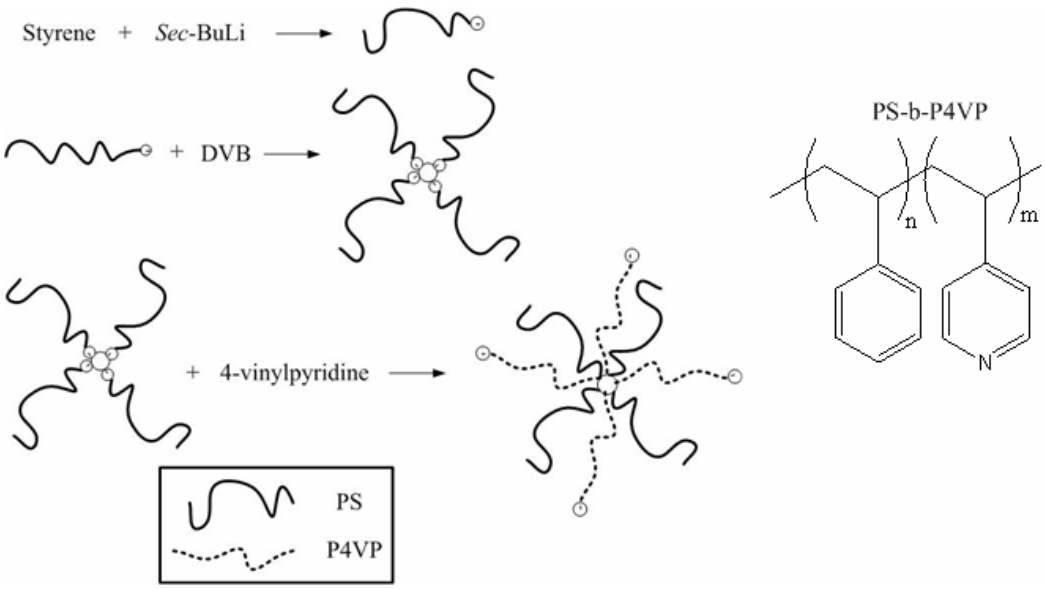

Figure 1-1 Synthesis of hetero-arm star PS-*b*-P4VP.

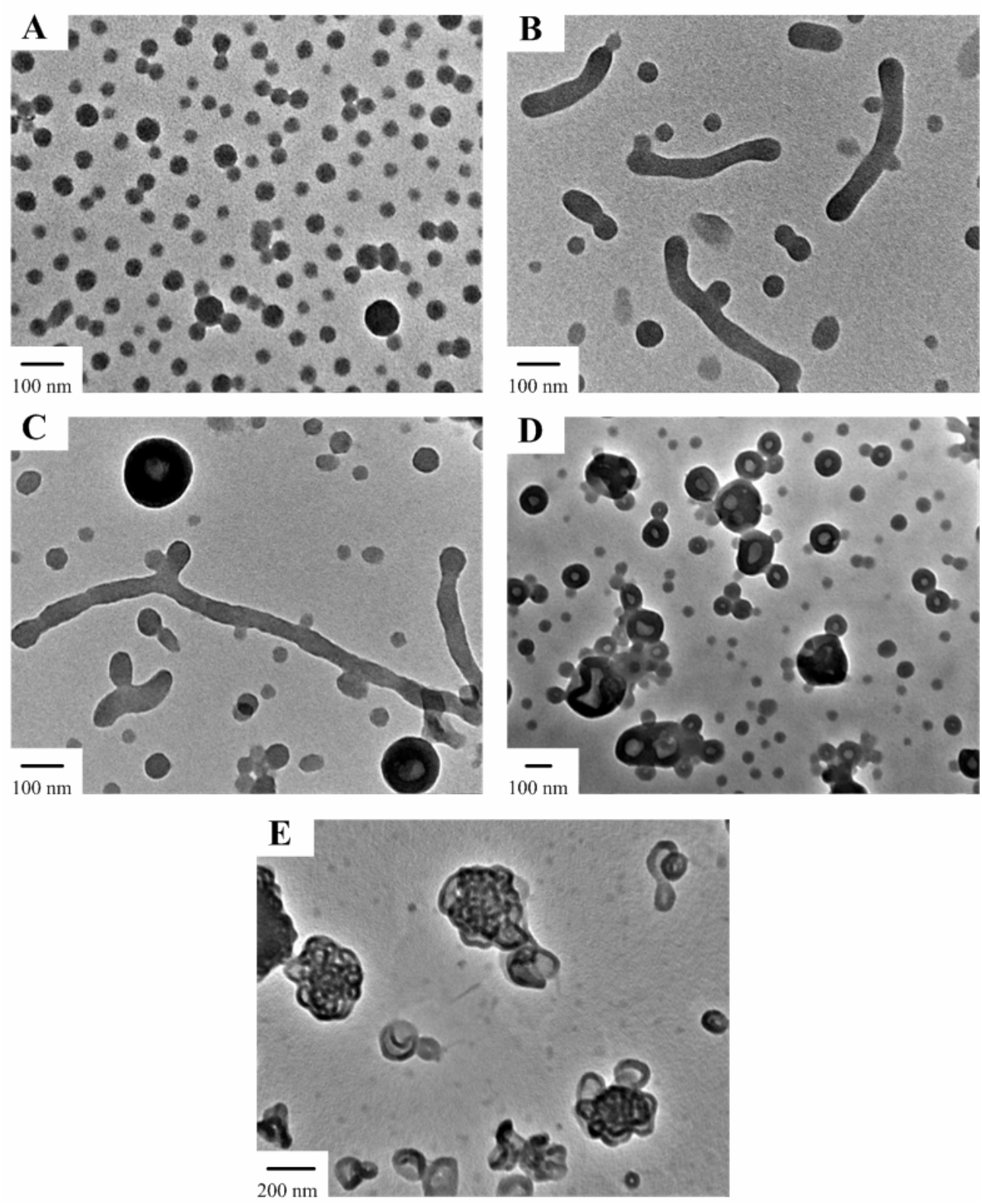

Figure 1-2. Morhological transition with varying water content in water/DMF system: (A) a pure sphere morphology at 5.7 wt% water; (B) a mixed spheres and cylinders at 8.3 wt% water;(C) a mixed cylinders and vesicles at 10.9 wt% water; (D) a pure vesicles at 13.5 wt% water; (E) large compound vesicles at 16.1 wt%.

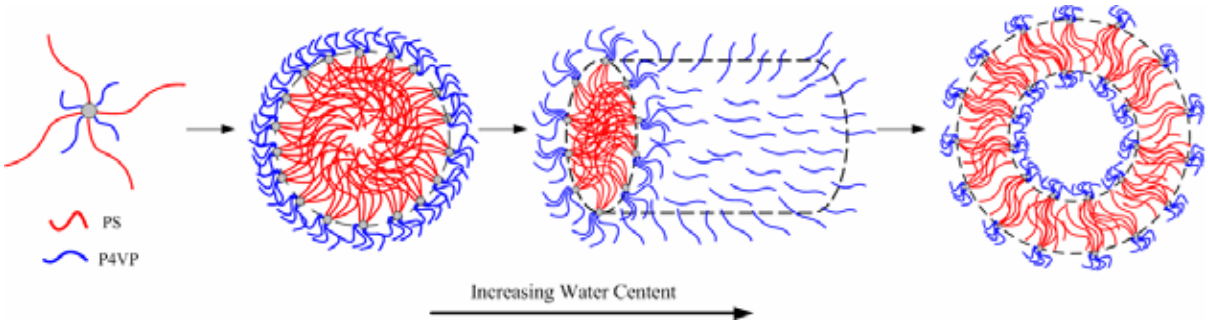

Figure 1-3. Schematic illustration of morphological transformation of PS_4-$P4VP_4$ induced by varying water content.

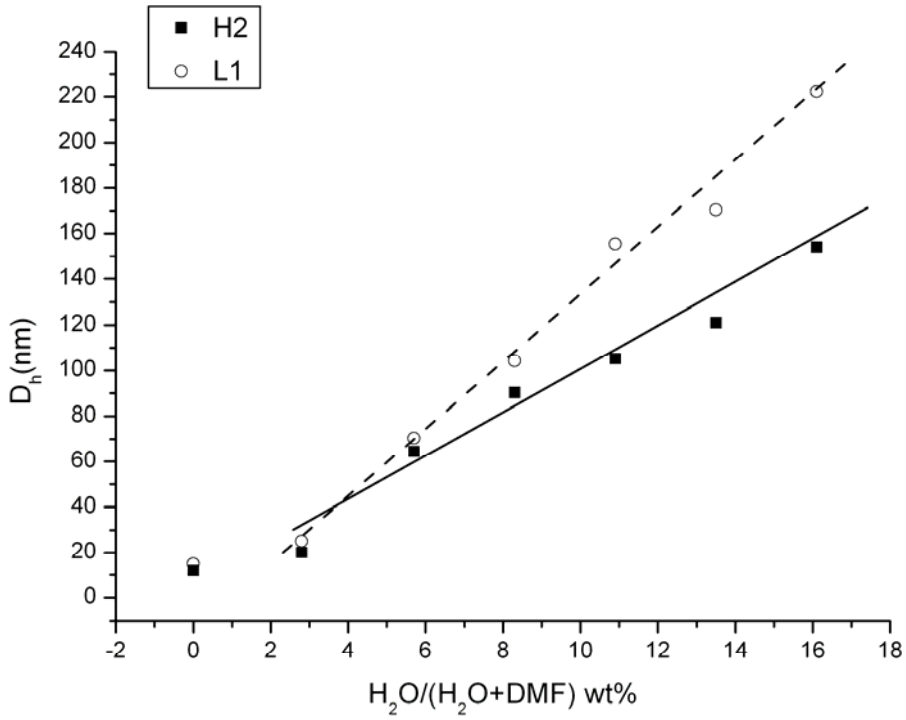

Figure 1-4. Variation of the hydrodynamic diameter as a function of the water content in water/DMF mixed solvent detected by DLS.

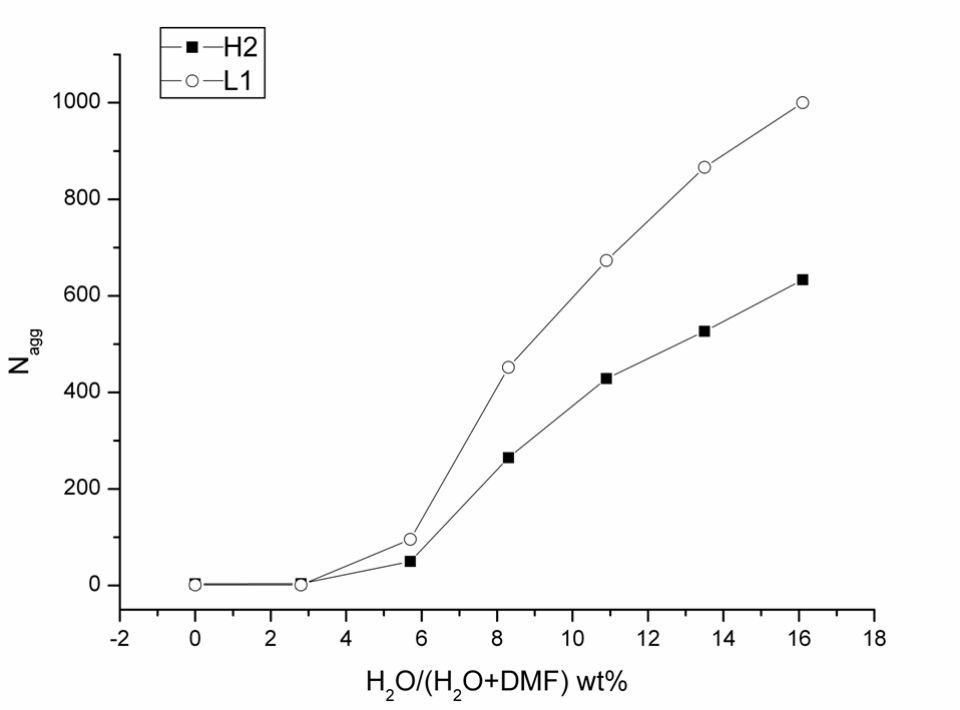

Figure 1-5. Variation of the aggregation numbers as a function of the water content in water/DMF mixed solvent detected by SLS.

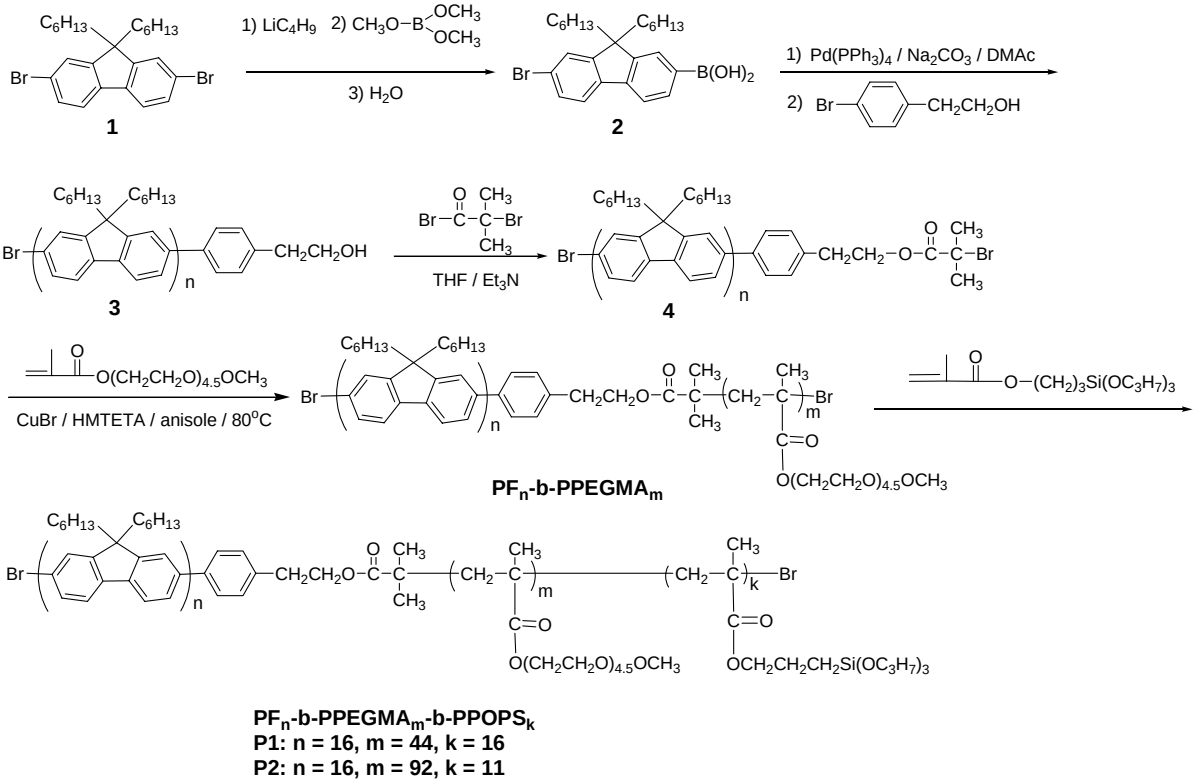

Figure 2-1. Synthetic Scheme of PF-PPEGMA-PPOPS.

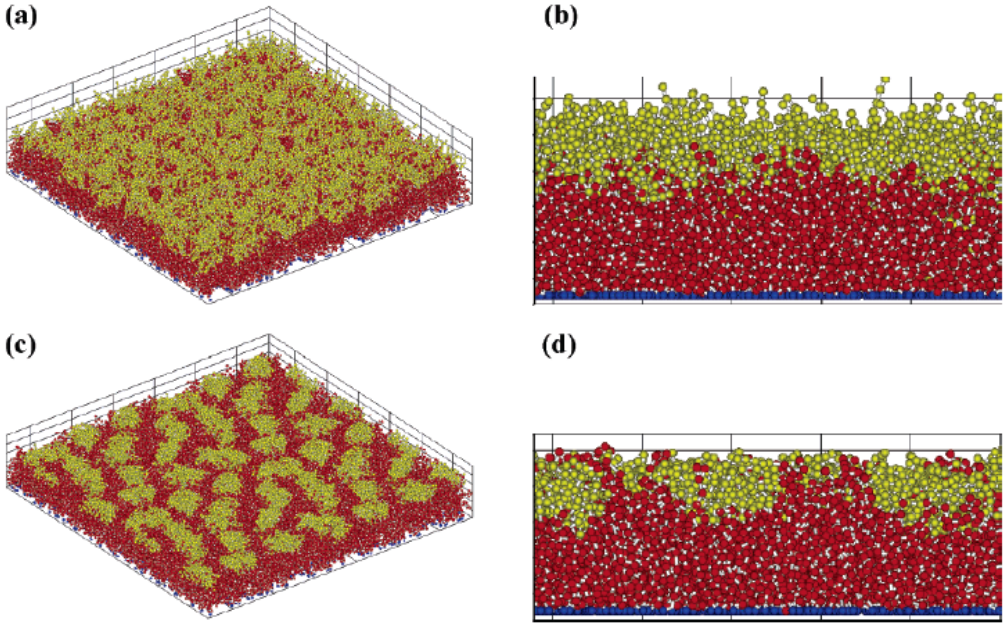

Figure 2-2. Simulated surface structures of rod-coil block copolymer brushes with the parameters of ρ_S= 0.7, n_A = 5, n_B =20, aBS = 26,and aAB= 40: (a) top view (for a_{AS} = 26); (b) side view (for a_{AS} = 26); (c) top view (for a_{AS}＝40); and (d) side view (for aAS= 40).The yellow and red spheres correspond to the rod and coil blocks, respectively. The blue spheres are the anchoring points of the copolymers on the surface. The system volume is set to be V=L_xˣL_yˣL_z) 30ˣ30ˣ20.

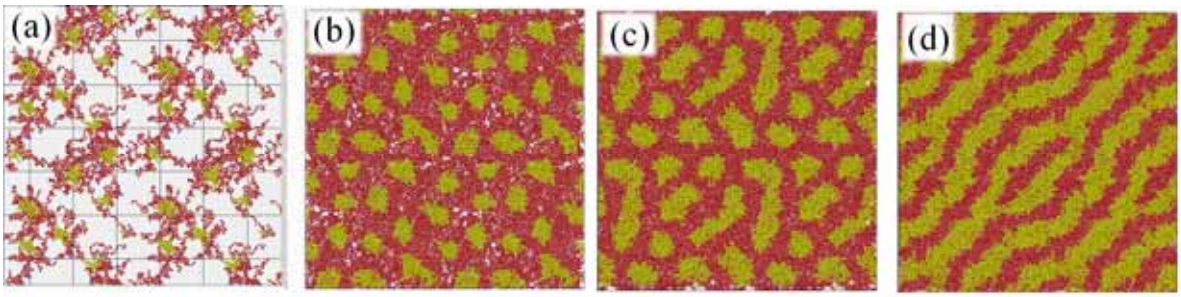

Figure 2-3. Top views of the surface structures of rod-coil block copolymer brushes. (a) ρ_S = 0.1; (b) ρ_S = 0.5; (c) ρ_S = 0.7; (c) ρ_S = 0.9.

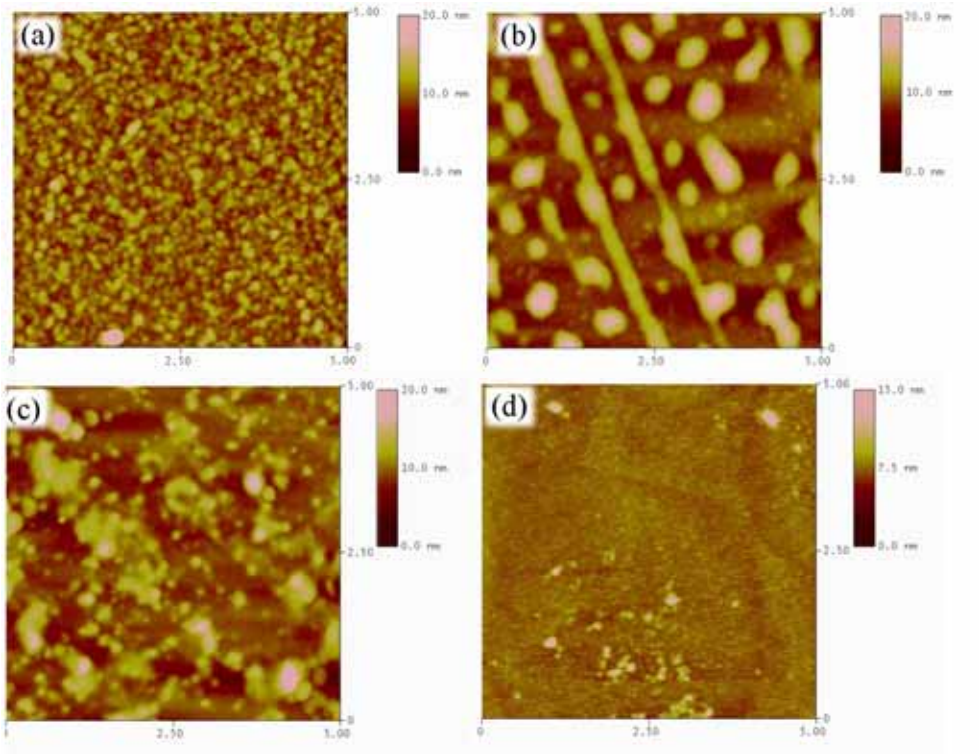

Figure 2-4. AFM images (5 × 5 μm) of the polymer brushes after solvent treatment. (a): **PB1** after toluene treatment; (b): **PB1** after methanol treatment; (c) and (d): **PB2** and **PB3** after methanol treatment.

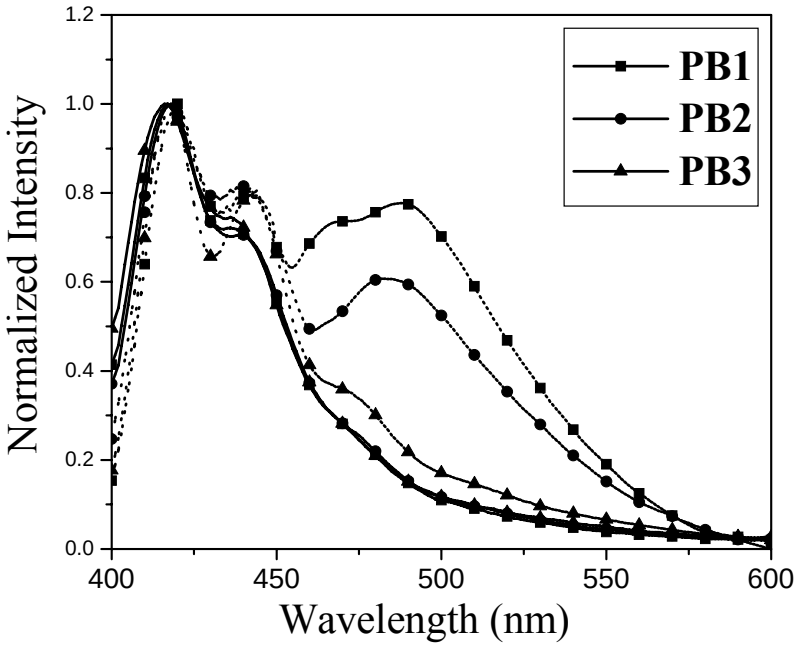

Figure 2-5. Photoluminescence spectra of polymer brushes after toluene treatment (solid lines) and methanol treatment (dot lines).

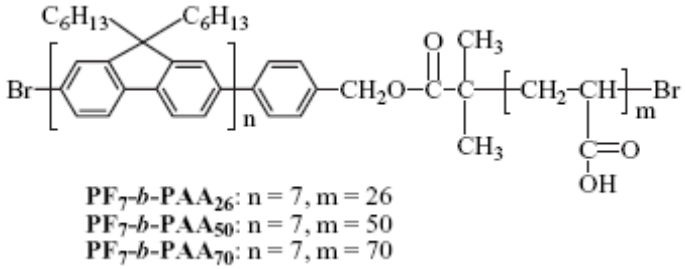

PF_7-*b*-PAA_{26}: n = 7, m = 26
PF_7-*b*-PAA_{50}: n = 7, m = 50
PF_7-*b*-PAA_{70}: n = 7, m = 70

Figure 3-1. Chemical structure of **PF-*b*-PAA** rod-coil diblock copolymers

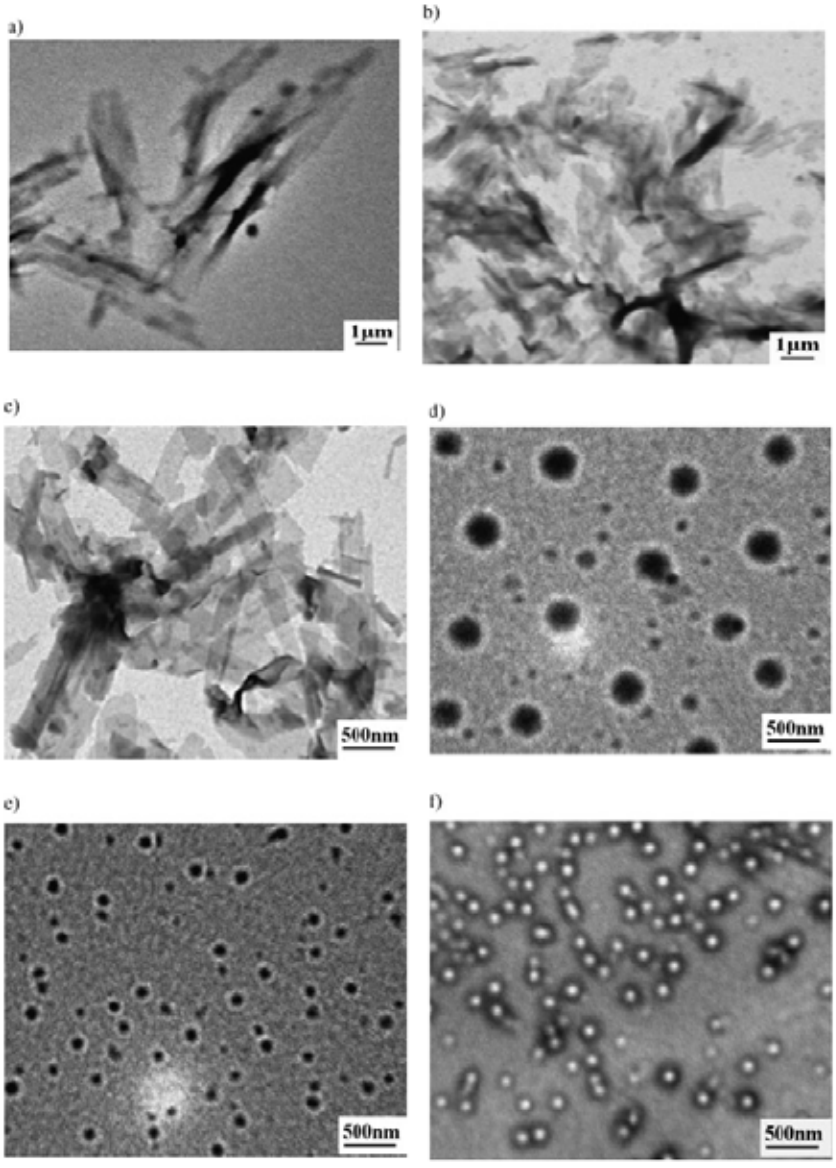

Figure 3-2. TEM images of **PF_7-*b*-PAA_{26}** [(a) to (c)] and **PF_7-*b*-PAA_{50}** [(d) to (f)] aggregates in dilute solution of DCM and methanol with methanol contents of (a), (d): 10 vol %; (b), (e): 25 vol %; and (c), (f): 50 vol %, respectively.

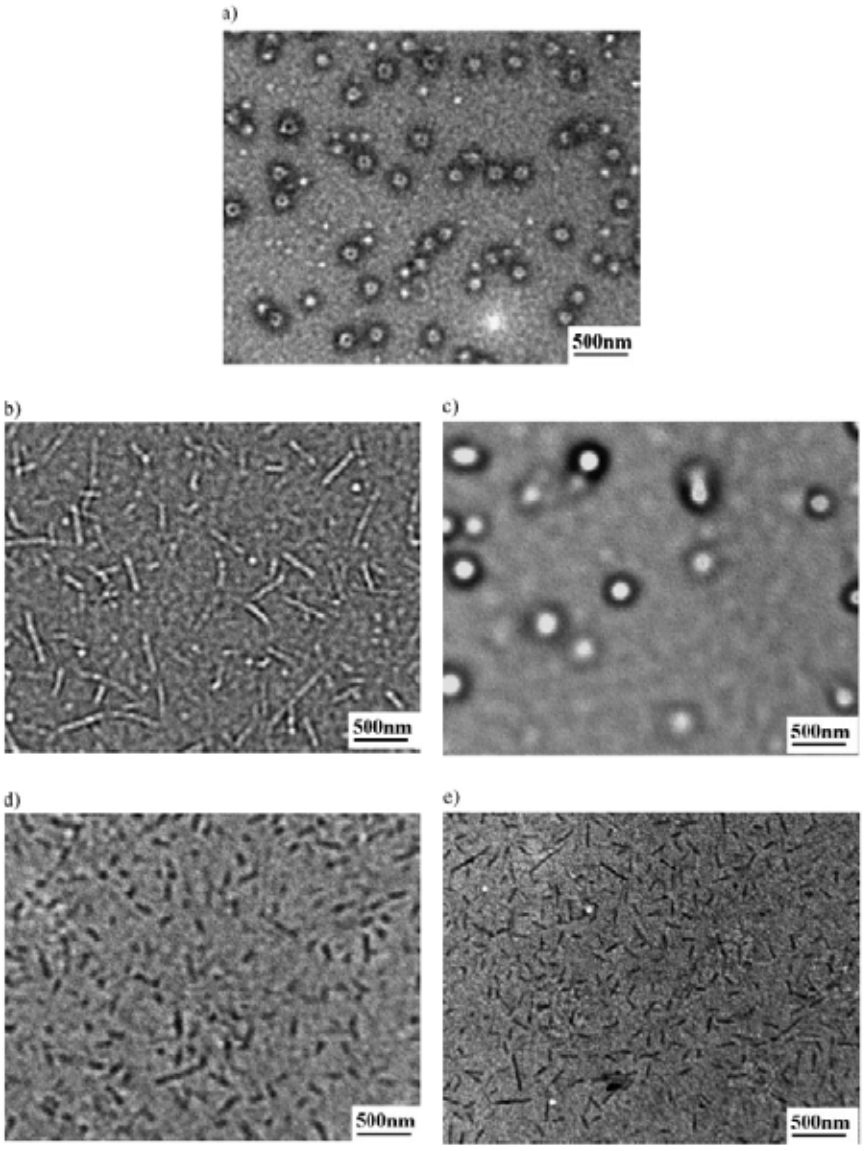

Figure 3-3. TEM images of **PF_7-*b*-PAA_{70}** aggregates in dilute solution of DCM and methanol with methanol contents of (a): 10 vol %, (b): 25 vol %, (c): 50 vol %, (d): 75 vol %, and (e): 90 vol % respectively.

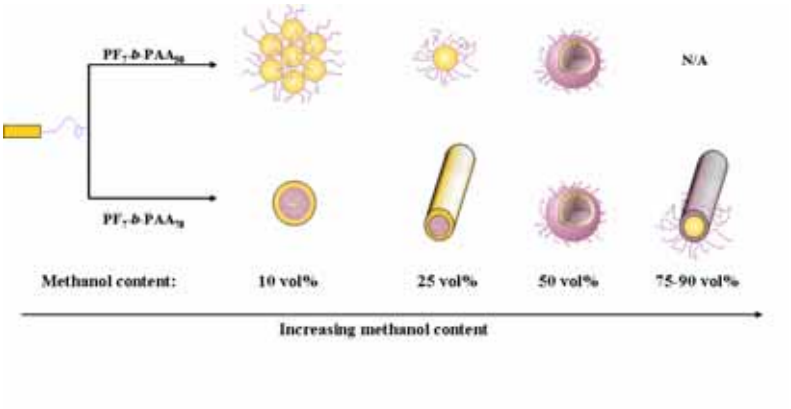

Figure 3-4. Schematic of the morphological transformation of **PF_7-*b*-PAA_{50}** and **PF_7-*b*-PAA_{70}**.

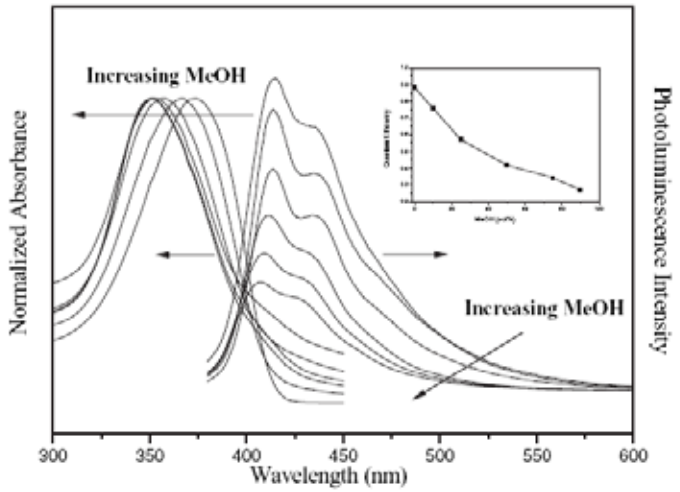

Figure 3-5. Optical absorption and photoluminescence spectra of **PF_7-b-PAA_{70}**. The inset shows the variation of PL quantum efficiency with methanol content.

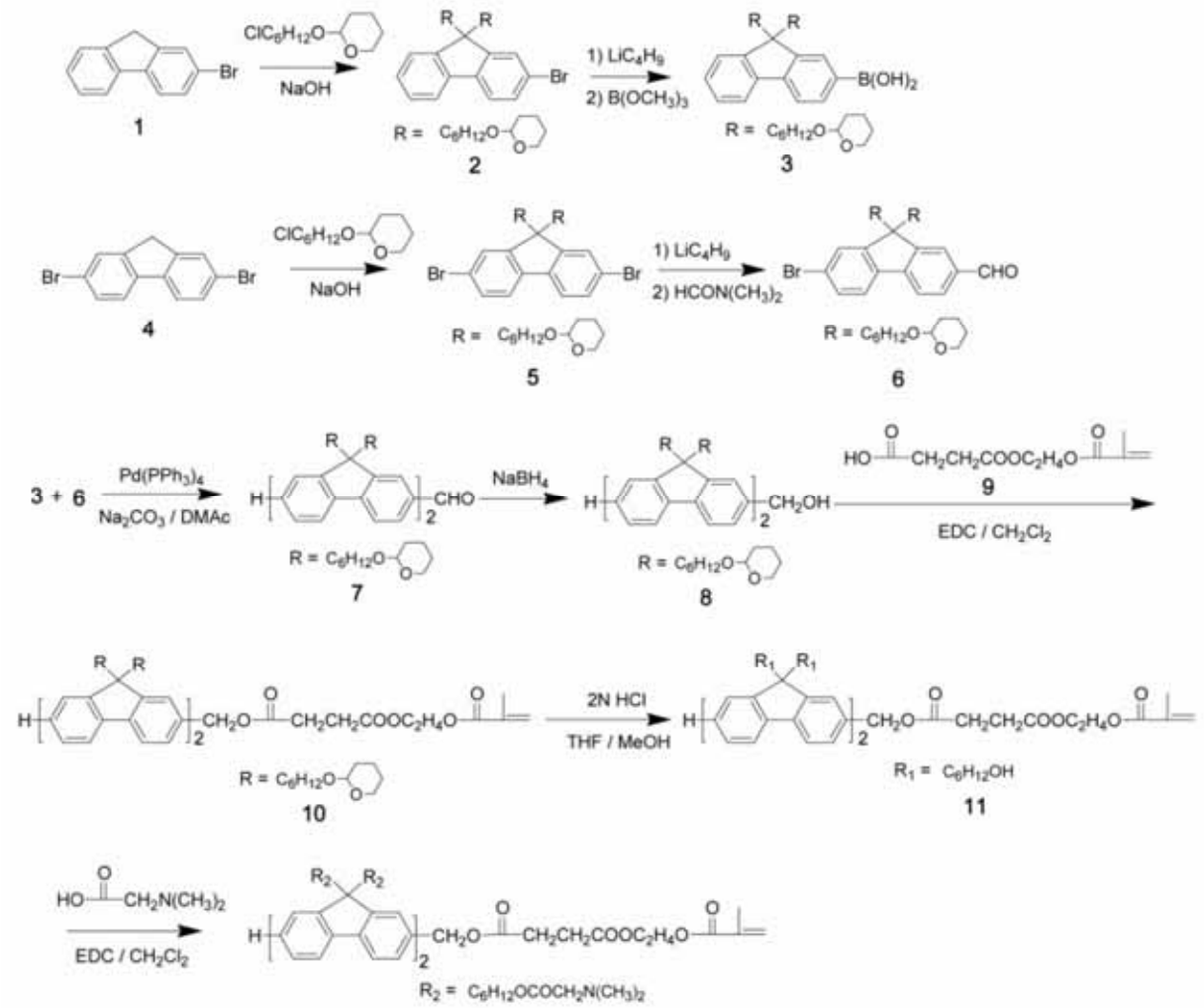

Figure 4-1. Synthesis of a new fluorene monomer.

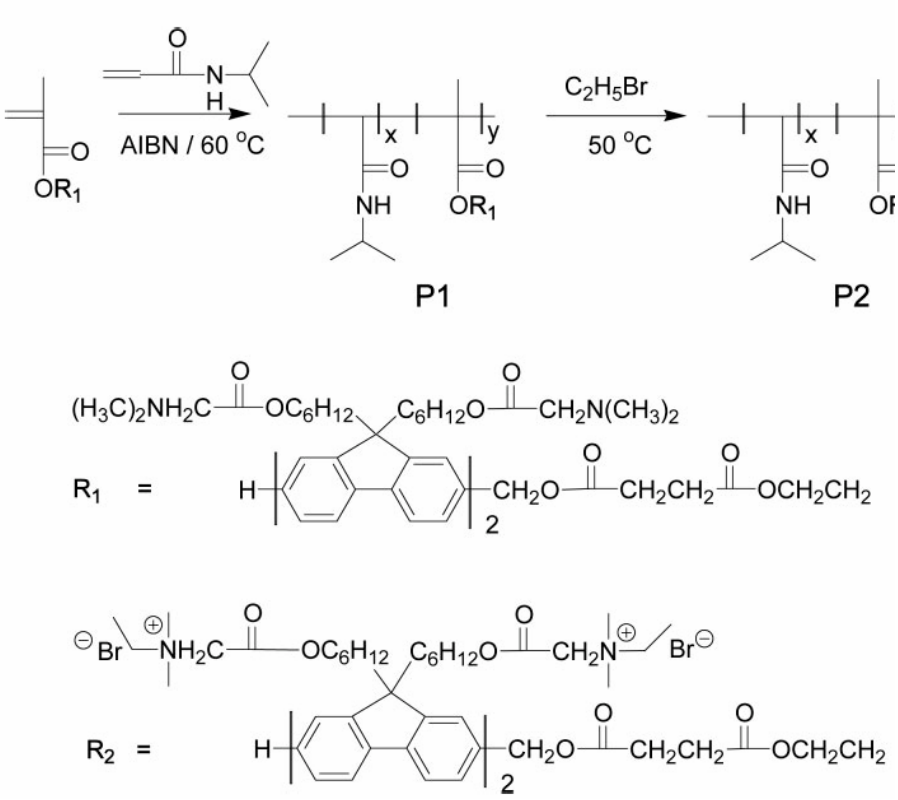

Figure 4-2. Preparation of **NIPAA** copolymers **P1** and **P2**.

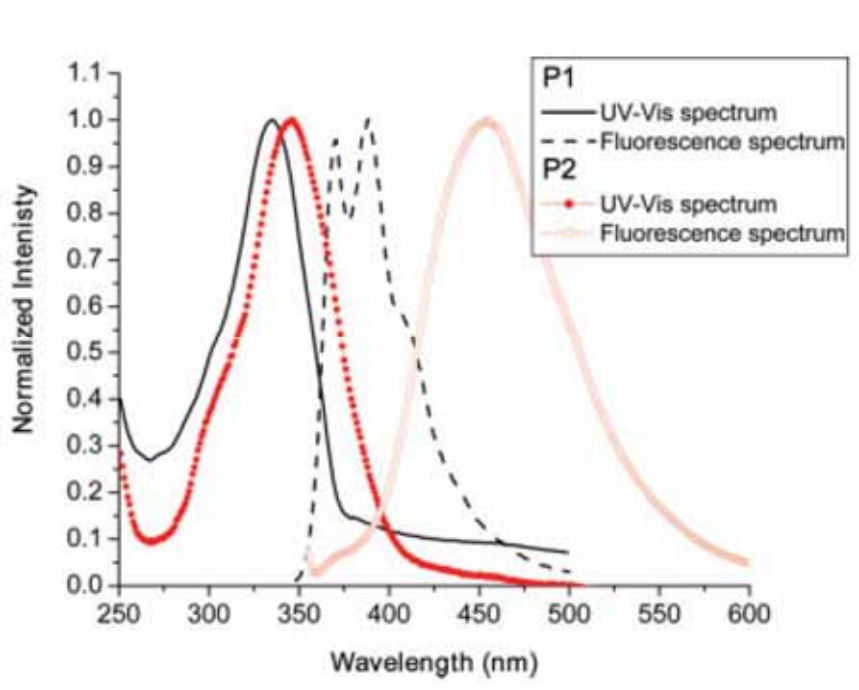

Figure 4-3. UV–vis absorption and fluorescence spectra of **P1** and **P2** in water. The excitation wavelength at 340 nm is the absorption maximum.

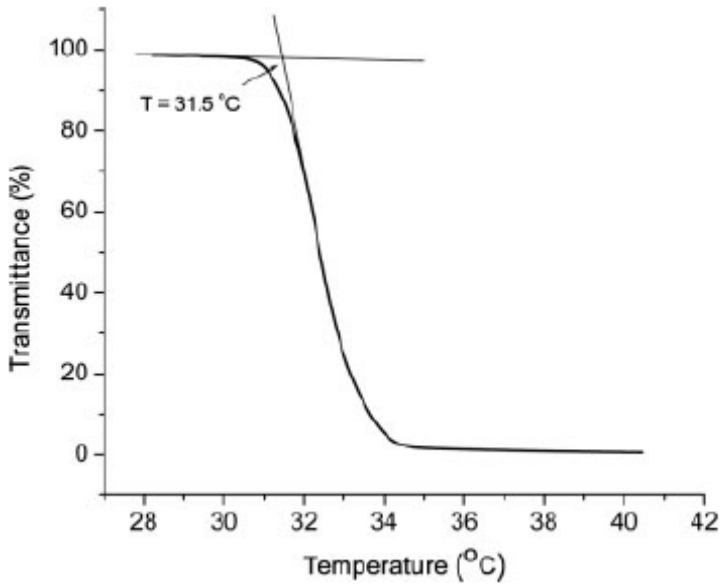

Figure 4-4. Optical transmittance spectrum of the prepared PNIPAA copolymer (P1) in an aqueous solution. The LCST was determined from the curve of the slope.

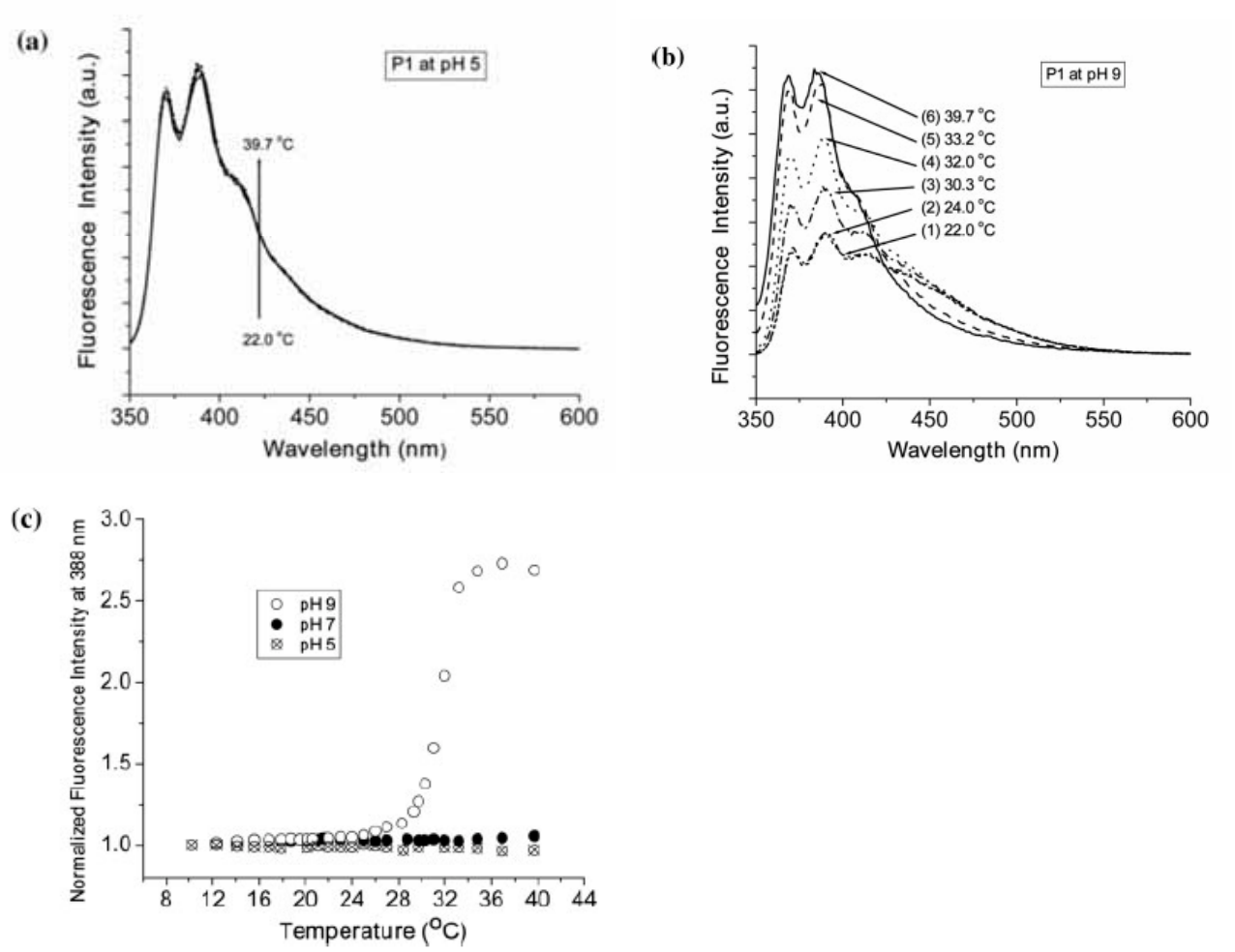

Figure 4-5. (a,b) Variation of the fluorescence intensity of copolymer **P1** in aqueous solutions with the temperatures and pH values [(a) pH 5 and (b) pH 9] and (c) variation of the normalized fluorescence intensity (IT/I10 8℃) at 388 nm for pH 5, pH 7, and pH 9. The excitation wavelength was 340 nm.

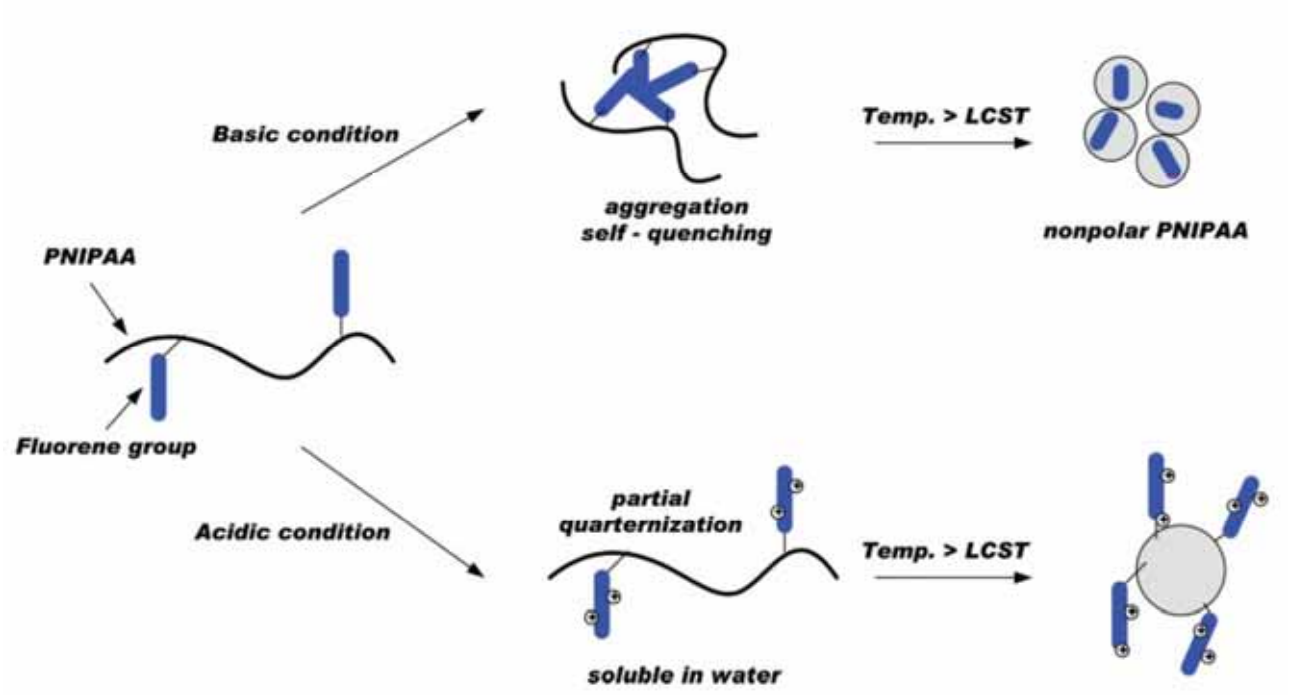

Figure 4-6. Proposed mechanism for the morphology of **P1** stimulated by the pH values and temperature.

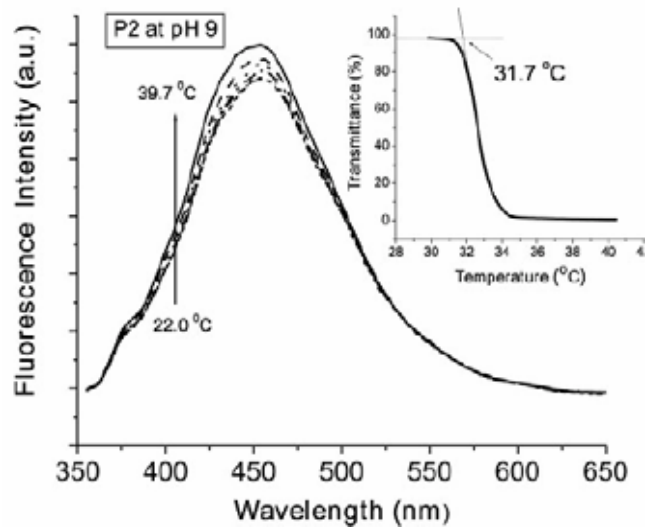

Figure 4-7. Variation of the fluorescence intensity of copolymer **P2** in aqueous solutions with different temperatures at pH 9. The excitation wavelength was 340 nm. The inset shows the optical transmittance spectrum of **P2** in water.

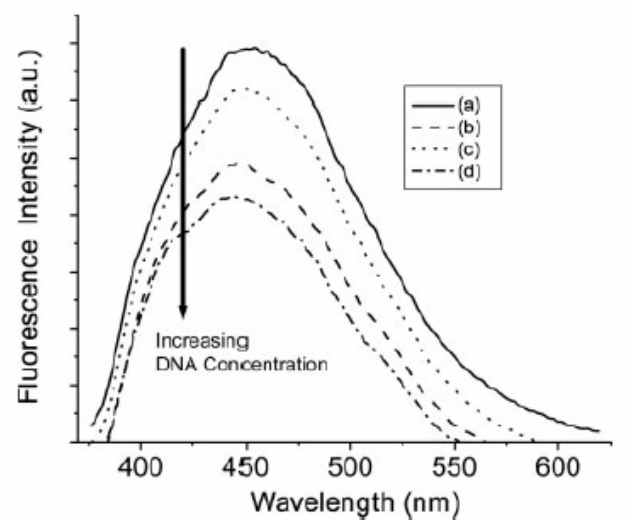

Figure 4-8. Sensing characteristics of **P2** with DNA in water solutions at pH 10: (a) pristine **P2** in 5.9 lM and (b–d) **P2** with the addition of 2.2, 4.5, and 5.2 nM DNA, respectively. The excitation wavelength was 340 nm.

.